LANGMUIR

Article

pubs.acs.org/Langmuir

Surface Decorating of $CH_3NH_3PbBr_3$ Nanoparticles with the Chemically Adsorbed Perylenetetracarboxylic Diimide

Ruimin Zhu,[†] Chengguang Gao,[†] Tingting Sun,[†] Li Shen,[‡] Dejun Sun,*[,†] and Xiyou Li*[,†,‡]

[†]Department of Chemistry, Shandong University, Jinan, Shandong 250100, China

[‡]College of Science, China University of Petroleum (East China), Qingdao, 266580, China

Supporting Information

ABSTRACT: An organic dye-modified organolead halide $CH_3NH_3PbBr_3$ nanoparticle (cubic) is prepared successfully by using a perylenetetracarboxylic diimide (PDI) bearing an $-NH_3^+$ headgroup as the capping ligand. The nanopartilces are homogeneous with high crystallinity. The photoluminescence of perovskite is quenched completely by the chemically adsorbed PDI molecules. This efficient fluorescence quenching has confirmed that the PDI molecules are anchored on the surface of $CH_3NH_3PbBr_3$ nanoparticle. The resulting nanoparticles can be dispersed in organic solvents, and the resulting dispersion remains stable for days. This result provides a general guideline for surface engineering of organolead halide $CH_3NH_3PbBr_3$ nanoparticles.

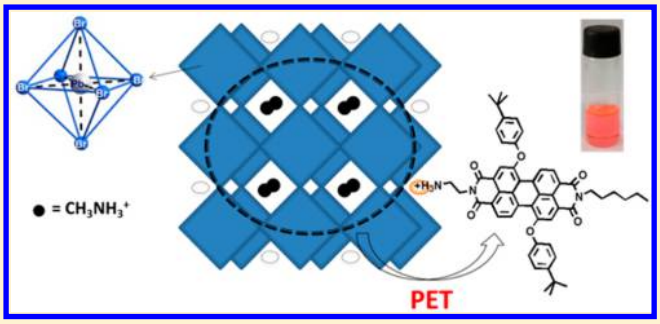

INTRODUCTION

Organometallic halide perovskite ABX_3 (A = organic cation, B = divalent/trivalent metal ion, X = halide anion) as an absorber in photovoltaic conversion devices has been triggered tremendous research interest in recent years, especially for $CH_3NH_3PbX_3$ (X = I or Br).[1−10] The power conversion efficiency of perovskite solar cells (PSCs) has been constantly raised from the initial 3.8%[1] to 20.2%[11] due to the large absorption coefficients,[12] small direct band gaps,[3] high charge-carrier mobilities[13,14] and long exciton diffusion length,[15,16] which makes PSCs the most powerful competitor for the next generation practical applicable solar cells. Interestingly, PSCs based on $CH_3NH_3PbBr_3$ has extremely high open-circuit voltage,[17−19] up to 2.2 V,[19] has been considered as a promising solar device to achieve water-electrolysis, and eventually realize the solar-to-hydrogen conversion. Moreover, the excellent properties of $CH_3NH_3PbX_3$ are also generating great research interest to explore the possible applications in other fields, such as light emitting diodes,[20,21] Li-ion batteries,[22] and fluorescence sensors and so on.[23]

To meet the needs of varied applications in different devices, $CH_3NH_3PbX_3$ materials have been prepared as bulky thin solid films,[3,11,15,16,19,20] confined nanomaterials in a nanoporous substrate.[1,2,4,17,18] Very recently, $CH_3NH_3PbBr_3$ nanoparticles (NPs) with sizes as small as several nanometers and high emission quantum yield have been prepared for the first time by replacing $CH_3NH_3^+$ on the periphery of the octahedron with octylammonium (OA) cations as the capping ligand.[24,25] The resulting NPs can be dispersed in toluene and keep stable for 24 h. Aggregation induced emission from $CH_3NH_3PbBr_3$ NPs dispersed in solution was found to be useful as fluorescence probe.[23] To make use of the advantages of the $CH_3NH_3PbBr_3$ NPs over bulky thin solid films,[25] and develop new applications for perovskite materials, further functionalization on the surface of the $CH_3NH_3PbBr_3$ NPs with other organic molecules should be a rational design. However, no such research has been reported so far. We presumed that by replacing the long alkyl amines with other organic photofunctional molecules, photoinduced electron transfer may occur between $CH_3NH_3PbBr_3$ and the anchored molecules, and thus the $CH_3NH_3PbX_3$ NPs could be endowed with new photofunctions, such as wider absorption spectrum, or novel emission properties.

Perylenetetracarboxylic diimides (PDIs), a special class of organic dyes with outstanding photochemical and photophysical property and photostability, are commonly applied in various optoelectronic devices as semiconductors or electron acceptors.[26−28] In addition, characteristic absorption of PDIs around 500−600 nm can make up for the low absorption of $CH_3NH_3PbBr_3$ at this range. Therefore, PDI molecules are ideal candidates to replace OA to be anchored on the surface of $CH_3NH_3PbBr_3$ NPs. In the present paper, we report for the first time PDI-modified $CH_3NH_3PbX_3$ NPs and the efficient photoinduced electron transfer between $CH_3NH_3PbX_3$ NP and anchored PDI molecules.

EXPERIMENTAL DETAILS

Material and Methods. All solvents were of analytical grade. DMF and acetone for preparation of perovskite NPs were dried by CaH_2 before use. All other chemicals were used as received without

Received: November 16, 2015
Revised: February 25, 2016
Published: March 13, 2016

DOI: 10.1021/acs.langmuir.5b04221
Langmuir 2016, 32, 3294−3299

Chart 1. Structures of PDI and PDI-C6

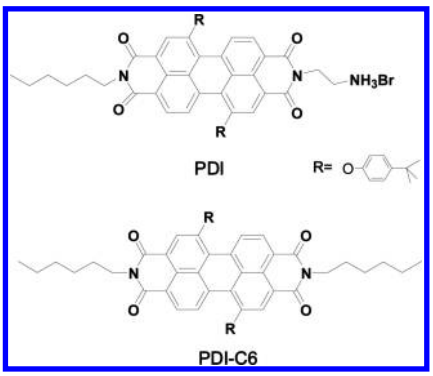

further purification. The initial material 3, 4, 9, 10-perylenetetracarboxylicacid dianhydride (96%) was purchased from commercial source.

Oleic acid (90 mg) in 2 mL octadecene were stirred and heated at 80 °C. Octylammonium bromide (0.03 mmol) and PDI (0.03 mmol) were added into the hot solution. Then methylammium bromide (4.4 mg, 0.04 mmol) in DMF (0.1 mL) and lead(II) bromide (36.7 mg, 0.1 mmol) in DMF (0.1 mL) were subsequently added. The pink precipitates (**PDI-P**$_{OA1}$) were formed by adding the hot reaction solution into hot acetone and centrifugated (7000 rpm, 10 min). The nanoparticles were washed by toluene to remove oleic acid and octadecene and then dried at room temperature.

Measurements. ^{1}H NMR spectra were recorded on a Bruker 400 MHz NMR spectrometer with chemical shifts reported in ppm (TMS as internal standard). Absorption spectra were measured on Shimadzu UV-2450 spectrophotometer. Steady-state fluorescence spectra were recorded on F-280 fluorescence spectrophotometer. Fluorescence quantum yields and nanosecond transient fluorescence spectra were collected on Edinburgh Instruments FLS920 three-monochromator spectrophotometer. The absolute fluorescence quantum yields were obtained by integrating sphere method and fluorescence decay was performed in the single photon counting (TCSPC) mode. Electrochemical measurements were carried out on CHI-760 electrochemical workstation in DMF containing 0.10 M tetra-*n*-butylammonium hexafluorophosphate ($(nBu)_4NPF_6$) as supporting electrolyte at a scan rate at 0.1 V/s. Typically, a conventional three-electrode cell was used with a platinum carbon working electrode, a platinum wire as the counter electrode and 0.01 M Ag/$AgNO_3$ as reference electrode. The cyclic differential pulse voltammogram data was collected after N_2 purging into the solution for about 10 min. Powder X-ray diffraction (XRD) patterns were obatained by D8 Advance X-ray diffractometer (Bruker, Germany) with Cu Ka radiation. High-resolution transmission electron mictroscopy (HRTEM) graphs were taken by JEM 2100 miroscope at an accelerating voltage of 200 kV. All the measurements were conducted at room temperature.

■ RESULTS AND DISCUSSIONS

Synthesis and Phase Analysis. Following the literature,[24] it is crucial to choose capping ligands with an appropriate length for the homogeneity of perovskite NPs. So **PDI** with an ethyleneamine headgroup on one side and a long alkyl tail on the other side has been designed. The ammonium group is expected to be able to anchor on the perovskite crystal surface. **PDI** (Scheme S1) was synthesized according to the reported methods,[29] and the details of the synthetic procedures and the molecular structure characterization are presented in the Supporting Information.

For comparison purposes, we have successfully repeated the preparation of $CH_3NH_3PbBr_3$ NPs capped by octylammonium bromide (**P**$_{OA}$).[24] The characterizations of **P**$_{OA}$ by absorption and photoluminescence (PL) spectra (see Figure S1), XRD, and HRTEM images are shown in the Supporting Information (see Figure S2). XRD patterns reveal the cubic phase for **P**$_{OA}$, and HRTEM images suggest that the crystalline surfaces of NPs are in good agreement with the results reported.[30] It should be noted that its absorption and photoluminescence bands in the spectra of **P**$_{OA}$ blue-shifted a little bit compared with that reported in the literature, which can be ascribed to the different size distribution of **P**$_{OA}$ from that of the literature (Figure S2).[31]

PDI-modified $CH_3NH_3PbBr_3$ NPs were prepared by partially or completely replacing octylammonium cations (OA) with **PDI** following the synthetic procedures of **P**$_{OA}$ (see Supporting Information). We have tried three different ratios between PDI and OA, 1/2, 1/1 and 1/0. These samples are labeled as **PDI-P**$_{OA2}$, **PDI-P**$_{OA1}$, and **PDI-P**, respectively. Figure 1 shows their

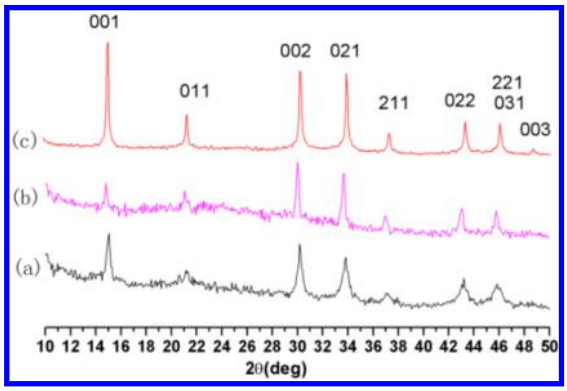

Figure 1. X-ray diffraction patterns of $CH_3NH_3PbX_3$ NPs. (a) **P**$_{OA}$ (b) **PDI-P**, and (c) **PDI-P**$_{OA1}$.

XRD patterns. The diffraction pattern of **PDI-P**$_{OA2}$ is very similar to that of **PDI-P**$_{OA1}$ (Figure S3 in the Supporting Information), so only the diffraction patterns of **PDI-P**$_{OA1}$, and **PDI-P** are shown. The diffraction peaks agree well with that of **P**$_{OA}$, which can be assigned to the diffraction of cubic $CH_3NH_3PbBr_3$.[24] No impure diffraction peak is identified from the diffraction patterns of **PDI-P**$_{OA1}$ and **PDI-P**. HRTEM images as shown in Figure 2 reveal the same results. The measured lattice fringe spacings in Figure 2b,c are 0.243 and 0.268 nm, corresponding to (211) and (021) family planes of

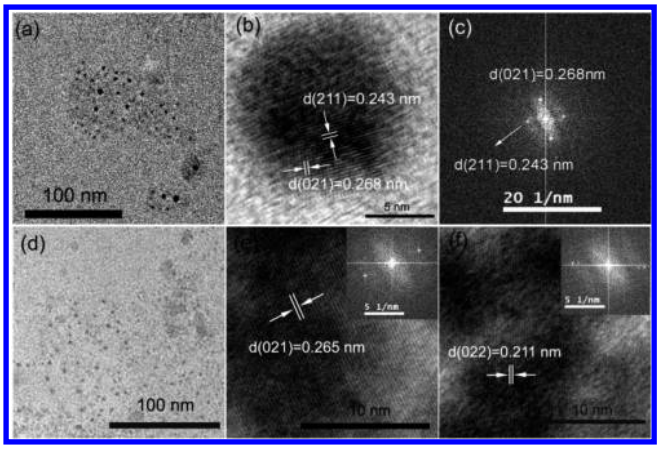

Figure 2. HRTEM images and the corresponding FFT analysis of **PDI-P**$_{OA1}$ and **PDI-P** NPs: (a) view of **PDI-P**$_{OA1}$ NPs; (b,c) lattice fringe phase and its FFT analysis of **PDI-P**$_{OA1}$; (d) view of **PDI-P** NPs; (e,f) lattice fringe phase of **PDI-P** and their FFT analysis (insets).

DOI: 10.1021/acs.langmuir.5b04221
Langmuir 2016, 32, 3294−3299

cubic $CH_3NH_3PbBr_3$.[30,32] Moreover, the *a*-lattice parameters calculated from these *d*-spacing data with the function of $1/d^2_{hkl} = (h^2 + k^2 + l^2)/a^2$ are 5.97 ± 0.02 and 5.94 ± 0.02 Å for **PDI-P$_{OA1}$** and **PDI-P**, respectively, which are also in good accordance with cubic $CH_3NH_3PbBr_3$ with $Pm\bar{3}m$ space group.[30,32] Energy dispersive spectrometer analysis (EDS)-(Figure S4) for **PDI-P$_{OA1}$** shows Pb:Br:O = 1:3.18:1.8. It means that the ratio of PDI and $CH_3NH_3PbBr_3$ is 0.3:1 in **PDI-P$_{OA1}$**. Similar EDS analysis reveals that the ratio between PDI and $CH_3NH_3PbBr_3$ in **PDI-P** is 0.6:1.

Steady-State Fluorescence Quenching. The absorption spectra of **PDI-P$_{OA1}$** and **PDI-P** are shown in the inset of Figure 3. The absorption spectrum of **PDI-P$_{OA1}$** was the

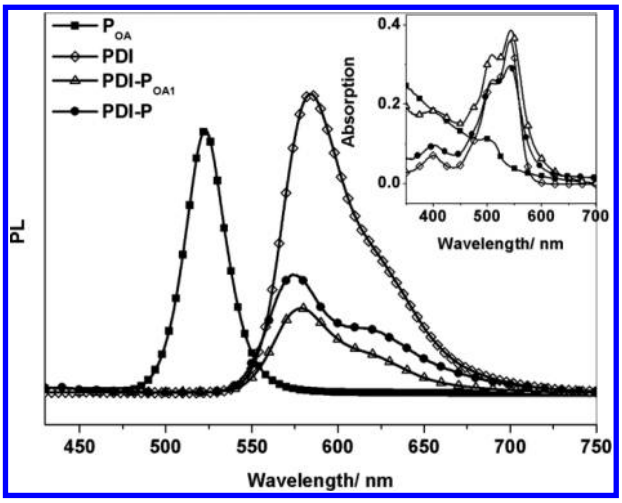

Figure 3. PL spectra of **PDI-P$_{OA1}$**, **PDI-P**, **P$_{OA}$**, and **PDI** excited at 401 nm. Inset shows the absorption spectra.

superposition of the absorption spectra of PDI and P_{OA}, which has also found for **PDI-P$_{OA2}$** (Figure S5 in the Supporting Information). However, the absorption spectrum of **PDI-P** reveals distinctive change on the 0−0/0−1 peak ratio with respect to that of pure **PDI** and **PDI-P$_{OA1}$**, which can be attributed to the formation of PDIs aggregates in **PDI-P** NPs.[29]

Figure 3 compares the steady state PL spectra of **PDI-P$_{OA1}$** with that of **P$_{OA}$** and **PDI** with excitation at 401 nm. In toluene, the characteristic emission of **P$_{OA}$** appears at 523 nm, which is similar to that reported in literature.[24] However, this emission band disappears in the spectrum of **PDI-P$_{OA1}$**. A broad emission band appears around 580 nm, which can be assigned to the fluorescence of **PDI**.[33] As revealed by the absorption spectra, inset of Figure 3a, both **P$_{OA}$** and **PDI** can absorb light at the excitation wavelength (401 nm), therefore, the emission peaks of both **PDI** and **P$_{OA}$** should be observed in the fluorescence spectrum of **PDI-P$_{OA1}$**. The missing of the emission of **P$_{OA}$** suggests that it has been quenched by **PDI** with an efficiency of 100%. In the PL spectrum of **PDI-P**, the emission of **P$_{OA}$** disappears too, indicating the presence of similar efficient fluorescence quenching with that in **PDI-P$_{OA1}$**. Similar results are also found in the PL spectrum of **PDI-P$_{OA2}$** (Figure S6 in the Supporting Information).

Because the emission of **P$_{OA}$** overlaps well with the absorption of **PDI** (Figure S7), energy transfer from **P$_{OA}$** to the **PDI** subunit within **PDI-P$_{OA1}$** was suspected to be the reason for the fluorescence quenching of **P$_{OA}$** by **PDI**. So the excitation spectrum of **PDI-P$_{OA1}$** by monitoring the emission of **PDI** at 576 nm was recorded (Figure S8). The excitation spectrum resembles the absorption spectrum of pure **PDI**, indicating that the absorption of **P$_{OA}$** in the range of 350−550 nm does not contribute to the fluorescence of **PDI** at 576 nm, which *excludes* the presence of energy transfer between excited **P$_{OA}$** and **PDI** within **PDI-P$_{OA1}$**.

Electrochemical Properties and Energy Level Diagrams. To explain the fluorescence quenching, redox potentials of pure **PDI** have been measured, and its HOMO and LUMO energy bands are calculated from the half-wave redox potentials (Figure S9 and Table 1). It is found that the

Table 1. Half-Wave Redox Potentials[a] (vs SCE) of PDI and PDI-C6 in DMF

compound	Ox_1	Red_1	E_{HOMO}/eV	E_{LUMO}/eV
PDI	1.36	−0.83	−5.80	−3.61
PDI-C6	1.33	−0.84	−5.77	−3.60

[a]Value obtained by DPV in dry DMF with 0.1 M $(nBu)_4NPF_6$ as the supporting electrolyte and Fc/Fc^+ as an internal standard.[29]

HOMO and LUMO energy levels of PDI match well with the covalent band (VB) and conduction band (CB) of $CH_3NH_3PbBr_3$ NPs (Figure 4),[34] respectively. The electron

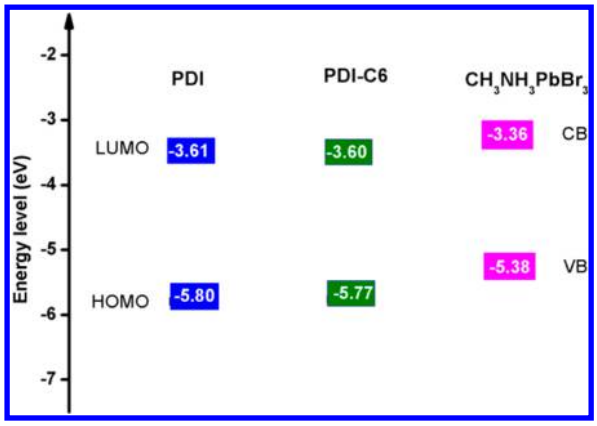

Figure 4. Energy level diagram of **PDI**, **PDI-C6**, and $CH_3NH_3PbBr_3$. The CB and VB of $CH_3NH_3PbBr_3$ were quoted from the literature.[34]

injection from the CB of $CH_3NH_3PbBr_3$ to the LUMO of **PDI** is thermodynamically favorable, which may responsible for the fluorescence quenching of **P$_{OA}$** by PDI subunit within **PDI-P$_{OA1}$** when **P$_{OA}$** subunit is excited.

Comparison with PDI-C6. To confirm that the significant fluorescence quenching between **P$_{OA}$** and **PDI** subunits within these three samples is caused by the anchoring of ammonium group of **PDI** on the surface of $CH_3NH_3PbBr_3$ NP rather than by the physically adsorbed **PDI** molecules, we use another **PDI** derivatives, **PDI-C6**, without the valid anchor $-NH_3^+$, instead of **PDI** in **PDI-P$_{OA1}$**. The resulting product was labeled as **PDI-C6/P$_{OA}$**. The absorption and PL spectra are shown in Figure 5. The absorption spectrum of **PDI-C6/P$_{OA}$** is the superposition of the absorption spectrum of pure **PDI** and **P$_{OA}$**. The PL spectrum of **PDI-C6/P$_{OA}$** presents two bands at 521 and 575 nm, which can be assigned to the emission of **P$_{OA}$** and **PDI**, respectively.[24,29] Obviously, the emission from **P$_{OA}$** has not been quenched, or at least has not been completely quenched. This is contrary to the PL spectrum of **PDI-P$_{OA2}$**, **PDI-P$_{OA1}$**, and **PDI-P** as mentioned above. This result indicates that the **PDI-C6** molecules cannot anchor onto the surface of **P$_{OA}$** due

DOI: 10.1021/acs.langmuir.5b04221
Langmuir 2016, 32, 3294−3299

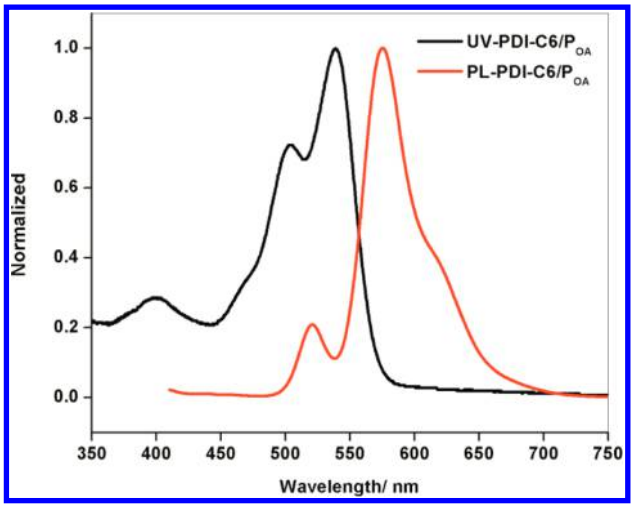

Figure 5. Absorption and PL spectra of **PDI-C6/P$_{OA}$** in toluene.

to the missing of ammonium cation headgroup, and therefore the emission of the **P$_{OA}$** subunit cannot be quenched, or at least completely quenched.

Photoluminescence Dynamics. The difference between **PDI-C6/P$_{OA}$** and **PDI-P$_{OA1}$** was also revealed by the time-resolved PL dynamics. The decay kinetics of the emission of **PDI-P$_{OA1}$** and **PDI-C6/P$_{OA}$** at 523 nm is compared with that of pure **P$_{OA}$** in Figure 6. The fluorescence decay dynamics of

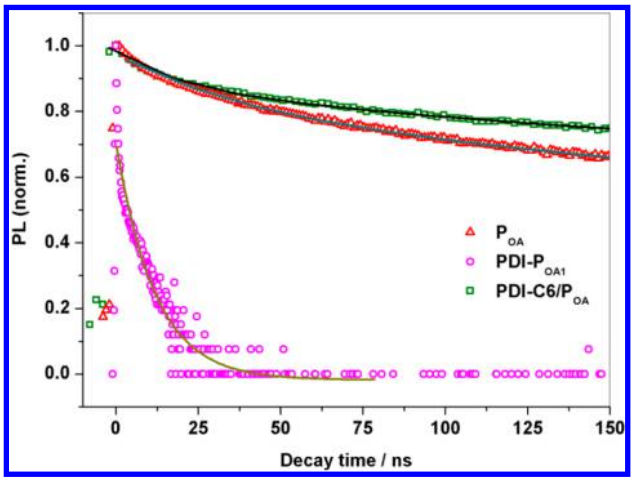

Figure 6. Time-resolved PL dynamics of $CH_3NH_3PbBr_3$ NPs in toluene probed at 523 nm after excitation at 370 nm.

PDI-P$_{OA1}$ is significantly faster than that of **PDI-C6/P$_{OA}$**. The fitting of the decay curve of the pure **P$_{OA}$** gives three lifetimes (Table 2): 17.6, 76.8, and 320 ns. The 76.8 ns component dominates (46.5%) the decay. The lifetime of the long-lived component (320 ns) is close to that of $CH_3NH_3PbI_{3-x}Cl_x$ film.[16] Similar three lifetimes are deduced from the decay of **PDI-C6/P$_{OA}$**, but the component with the longest lifetime dominates the decay. The proportion of the short lifetime components (τ_1 and τ_2) in the total emission of **PDI-C6/P$_{OA}$** decreases obviously, while that of the long lifetime component increases. Based on the fact that the total fluorescence quantum yield of **PDI-C6/P$_{OA}$** is smaller than that of **P$_{OA}$**, the proportion decrease of the short lifetime components in the total fluorescence of **PDI-C6/P$_{OA}$** should be the result of the fluorescence quenching caused by **PDI-C6**. The fluorescence decay of PDI-C6/P$_{OA}$ as shown in Figure 6 is slower than that of pure **P$_{OA}$**, suggesting the decrease on the concentration of surface defects in **PDI-C6/P$_{OA}$** than in **P$_{OA}$**.[25] Moreover, because **PDI-C6** do not has anchoring group $-NH_3^+$, it can only physically adsorbed on the surface of perovskite NPs. So we suggest that the short-lifetime components in the emission of **P$_{OA}$** might belong to some defect states. The component has the longest lifetime that can be attributed to hole−electron pair recombination, which is the intrinsic lifetime of **P$_{OA}$**, and is found in many different perovskite NPs.[25] An extremely short lifetime (0.044 ns) was deduced from the decay dynamics. Because this value is close to the lower limit for the lifetime measurement of the instrument, it is not accurate and just qualitatively suggests the presence of efficient fluorescence quenching of **P$_{OA}$** by **PDI** within **PDI-P$_{OA1}$**. Similarly fluorescence decay dynamic is found for **PDI-P$_{OA2}$** (Figure S10 in the Supporting Information). The fitting results are also summarized in Table 2. Very short lifetimes were deduced, and the efficient fluorescence quenching was proved. This result corresponds well to the result of steady state fluorescence experiments as mentioned above. This significant difference in the PL decay dynamics between **PDI-P$_{OA1}$** (or **PDI-P$_{OA2}$**) and **PDI-C6/P$_{OA}$** reveal that the interaction between **PDI** and **P$_{OA}$** subunits within these two NPs are distinctively different. It is safe to conclude that **PDI** molecules with $-NH_3^+$ have anchored onto the surface of **P$_{OA}$**. It must be noted that we have also tried to record the fluorescence decay dynamics of **PDI-P**, the experiments did not lead to any reliable results. We attributed this result to the overwhelming emission of PDI caused by the large absorbance at the excitation wavelength, which overlaps with the emission of P$_{OA}$ at 523 nm. Due to the small content of PDI in **PDI-P$_{OA1}$**, the fraction of excitation light absorbed by PDI is small and the fluorescence of PDI should be not as strong as in that in **PDI-P**. So the fluorescence decay of **PDI-P$_{OA1}$** at 523 nm can be measured.

Following eq 1, we have also calculated the average fluorescence lifetimes (τ_{av}) for these materials, which correlated

Table 2. PL Decay of $CH_3NH_3PbBr_3$ NPs in Toluene Probed at 523 nm with Time Constant τ_i and Amplitude A_i

	P$_{OA}$	PDI-C6/P$_{OA}$	PDI-P$_{OA2}$	PDI-P$_{OA1}$
τ_1(ns) (A_1)	17.64 ± 0.34 (23.26%)	8.47 ± 0.19 (11.23%)	0.14 ± 0.004 (52.15%)	0.044 ± 0.002[b] (86.86%)
τ_2(ns) (A_2)	76.8 ± 1.47 (46.50%)	73.77 ± 1.17 (35.45%)	0.49 ± 0.01 (35.91%)	3.71 ± 0.05 (13.14%)
τ_3(ns) (A_3)	319.32 ± 5.60 30.25%)	389.57 ± 4.70 (53.32%)	4.51 ± 0.09 (11.93%)	-
χ^2	1.2	1.3	0.9	1.1
τ_{av}(ns)[a]	246.75	352.86	3.21	3.44
Φ_{PL}	0.522	0.424	0.091	0.141

[a]The total absolute fluorescence quantum yields including the emission of both **P$_{OA}$** and **PDI**. [b]This value is close to the lower limit for the lifetime measurement of the instrument, therefore, it is not accurate.

DOI: 10.1021/acs.langmuir.5b04221
Langmuir 2016, 32, 3294−3299

with the charge recombination time and the concentration of surface defects.[25]

$$\tau_{av} = \frac{A_1 t_1^{\ 2} + A_2 t_2^{\ 2} + \cdots + A_n t_n^{\ 2}}{A_1 t_{1+} A_2 t_{2+} \cdots + A_n t_n} \quad (1)$$

The long average lifetimes of $\mathbf{P_{OA}}$ and **PDI-C6/**$\mathbf{P_{OA}}$ evidenced the considerable reduction on the concentration of surface defects. Both **PDI-**$\mathbf{P_{OA2}}$ and **PDI-**$\mathbf{P_{OA1}}$ show average lifetimes around 3 ns, which significantly shorter than that of $\mathbf{P_{OA}}$ and **PDI-C6/**$\mathbf{P_{OA}}$, this can be attributed to electron transfer from $\mathbf{P_{OA}}$ to the adsorbed PDI molecules. There is no obvious difference between the τ_{av} of **PDI-**$\mathbf{P_{OA2}}$ and **PDI-**$\mathbf{P_{OA1}}$, which indicates that the short fluorescence lifetimes of them have nothing to do with the content of OA. Therefore, the very short τ_{av} is not caused by the reduction on the surface coverage of the perovskite NPs by OA.

Based on the experimental results as discussed above, the fluorescence quenching process within **PDI-**$\mathbf{P_{OA1}}$ and **PDI-C6/**$\mathbf{P_{OA}}$ can be illustrated by Figure 7. In **PDI-**$\mathbf{P_{OA1}}$, due to the presence of -NH_3^+ group, the **PDI** molecules can anchored to the surface of $\mathbf{P_{OA}}$ NPs firmly, resulting in a short distance between the **PDI** molecules and $\mathbf{P_{OA}}$ surface and then an efficient photoinduced electron transfer. However, in **PDI-C6/**$\mathbf{P_{OA}}$, the **PDI-C6** molecules can only be physically adsorbed on the surface of $\mathbf{P_{OA}}$ driven by the weak hydrophobic interactions between the long alkyl chains of **PDI-C6** and $\mathbf{P_{OA}}$. The distance between the molecules of **PDI-C6** and the surface of $\mathbf{P_{OA}}$ is large, so the fluorescence quenching is less efficient.

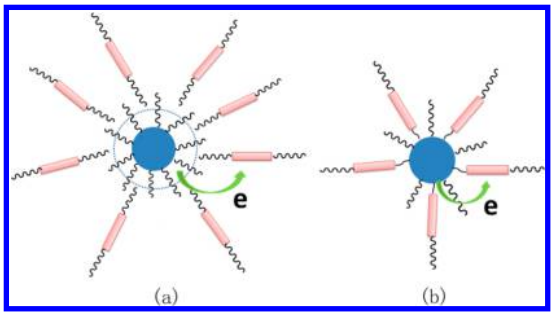

Figure 7. Illustration of electron transfer process: (a) **PDI-C6/**$\mathbf{P_{OA}}$ (b) **PDI-**$\mathbf{P_{OA1}}$. Note: The organic molecules were enlarged for clarity.

■ CONCLUSION

We have successfully synthesized **PDI**-modified $CH_3NH_3PbBr_3$ perovskite NPs for the first time. The resulted NPs can be dispersed in organic solvents. The dispersion can keep stable for several days. The anchored **PDI** molecules can quench the emission of $CH_3NH_3PbBr_3$ efficiently by photoinduced electron transfer from perovskite to **PDI**. Further studies on capping the surface of perovskite NPs with other organic dyes are going on in our lab.

■ ASSOCIATED CONTENT

Supporting Information

The Supporting Information is available free of charge on the ACS Publications website at DOI: 10.1021/acs.langmuir.5b04221.

A detailed synthesis of organic compounds, characterizations of $\mathbf{P_{OA}}$, differential pulse voltammetry (DPV), and steady-state and time-resolved spectra (PDF)

■ AUTHOR INFORMATION

Corresponding Author

*E-mail: xiyouli@sdu.edu.cn.

Notes

The authors declare no competing financial interest.

■ ACKNOWLEDGMENTS

We acknowledge the financial support from the National Natural Science Foundation of China (Grant Nos. 21173136 and 91233108) and the National Basic Research Program of China (973 Program: 2012CB93280).

■ REFERENCES

(1) Kojima, A.; Teshima, K.; Shirai, Y.; Miyasaka, T. Organometal Halide Perovskites as Visible-Light Sensitizers for Photovoltaic Cells. *J. Am. Chem. Soc.* **2009**, *131*, 6050−6051.

(2) Im, J.-H.; Lee, C.-R.; Lee, J.-W.; Park, S.-W.; Park, N.G. 6.5% Efficient Perovskite Quantum-Dot-Sensitized Solar Cell. *Nanoscale* **2011**, *3*, 4088−4093.

(3) Kim, H.-S.; Lee, C.-R.; Im, J.-H.; Lee, K.-B.; Moehl, T.; Marchioro, A.; Moon, S.-J.; Humphry-Baker, R.; Yum, J.-H.; Moser, J. E.; Grätzel, M.; Park, N.-G. Lead Iodide Perovskite Sensitized All-Solid-State Submicron Thin Film Mesoscopic Solar Cell with Efficiency Exceeding 9%. *Sci. Rep.* **2012**, *2*, 591.

(4) Lee, M. M.; Teuscher, J.; Miyasaka, T.; Murakami, T. N.; Snaith, H. J. Efficient Hybrid Solar Cells Based on Meso-Superstructured Organometal Halide Perovskites. *Science* **2012**, *338*, 643−647.

(5) Hodes, G. Perovskite-Based Solar Cells. *Science* **2013**, *342*, 317−318.

(6) Snaith, H. J. Perovskites: The Emergence of a New Era for Low-Cost, High-Efficiency Solar Cells. *J. Phys. Chem. Lett.* **2013**, *4*, 3623−3630.

(7) Park, N.-G. Organometal Perovskite Light Absorbers Toward a 20% Efficiency Low-Cost Solid- State Mesoscopic Solar Cell. *J. Phys. Chem. Lett.* **2013**, *4*, 2423−2429.

(8) Gao, P.; Grätzel, M.; Nazeeruddin, M. K. Organohalide Lead Perovskites for Photovoltaic Applications. *Energy Environ. Sci.* **2014**, *7*, 2448−2463.

(9) Green, M. A.; Emery, K.; Hishikawa, Y.; Warta, W.; Dunlop, E. D. Solar Cell Efficiency Tables (Version 43). *Prog. Photovoltaics* **2014**, *22*, 1−9.

(10) Even, J.; Pedesseau, L.; Katan, C.; Kepenekian, M.; Lauret, J.-S.; Sapori, D.; Deleporte, E. Solid-State Physics Perspective on Hybrid Perovskite Semiconductors. *J. Phys. Chem. C* **2015**, *119*, 10161−10177.

(11) Yang, W. S.; Noh, J. H.; Jeon, N.-J.; Kim, Y. C.; Ryu, S.; Seo, J.; Seok, S., II High-Performance Photovoltaic Perovskite Layers Fabricated Through Intramolecular Exchange. *Science* **2015**, *348*, 1234−1237.

(12) Zhu, X.; Su, H.; Marcus, R. A.; Michel-Beyerle, M. E. Computed and Experimental Absorption Spectra of the Perovskite $CH_3NH_3PbI_3$. *J. Phys. Chem. Lett.* **2014**, *5*, 3061−3065.

(13) Giorgi, G.; Fujisawa, J.-I.; Segawa, H.; Yamashita, K. Small Photocarrier Effective Masses Featuring Ambipolar Transport in Methylammonium Lead Iodide Perovskite: A Density Functional Analysis. *J. Phys. Chem. Lett.* **2013**, *4*, 4213−4216.

(14) Mitzi, D. B. Templating and Structural Engineering in Organic−Inorganic Perovskites. *J. Chem. Soc., Dalton Trans.* **2001**, 1−12.

(15) Xing, G.; Mathews, N.; Sun, S.; Lim, S. S.; Lam, Y. M.; Grätzel, M.; Mhaisalkar, S.; Sum, T. C. Long-Range Balanced Electron- and Hole-Transport Lengths in Organic-Inorganic CH3NH3PbI3. *Science* **2013**, *342*, 344−347.

(16) Stranks, S. D.; Eperon, G. E.; Grancini, G.; Menelaou, C.; Alcocer, M. J. P.; Leijtens, T.; Herz, L. M.; Petrozza, A.; Snaith, H. J. Electron-Hole Diffusion Lengths Exceeding 1 Micrometer in an Organometal Trihalide Perovskite Absorber. *Science* **2013**, *342*, 341−344.

DOI: 10.1021/acs.langmuir.5b04221
Langmuir 2016, 32, 3294−3299

(17) Edri, E.; Kirmayer, S.; Cahen, D.; Hodes, G. High Open-Circuit Voltage Solar Cells Based on Organic-Inorganic Lead Bromide Perovskite. *J. Phys. Chem. Lett.* **2013**, *4*, 897−902.
(18) Ryu, S.; Noh, J. H.; Jeon, N. J.; Kim, Y. C.; Yang, W. S.; Seo, J.; Seok, S., II Voltage Output of Efficient Perovskite Solar Cells with High Open-Circuit Voltage and Fill Factor. *Energy Environ. Sci.* **2014**, *7*, 2614−2618.
(19) Heo, J. H.; Im, S. H. $CH_3NH_3PbBr_3$- $CH_3NH_3PbI_3$ Perovskite-Perovskite Tandem Solar Cells with Exceeding 2.2 V Open Circuit Voltage. *Adv. Mater.* **2015**, DOI: 10.1002/adma.201501629.
(20) Li, J.; Bade, S. G. R.; Shan, X.; Yu, Z. Single-Layer Light-Emitting Diodes Using Organometal Halide Perovskite/Poly(ethylene oxide) Composite Thin Films. *Adv. Mater.* **2015**, *27*, 5196−5202.
(21) Kumawat, N. K.; Dey, A.; Narasimhan, K. L.; Kabra, D. Near Infrared to Visible Electroluminescencent Diodes Based on Organometallic Halide Perovskites: Structural and Optical Investigation. *ACS Photonics* **2015**, *2*, 349−354.
(22) Xia, H.; Sun, W.; Peng, L. Hydrothermal Synthesis of Organometal Halide Perovskites for Li-ion Batteries. *Chem. Commun.* **2015**, *51*, 13787−13790.
(23) Niu, Y.; Zhang, F.; Bai, Z.; Dong, Y.; Yang, J.; Liu, R.; Zou, B.; Li, J.; Zhong, H. Aggregation-Induced Emission Features of Organometal Halide Perovskites and Their Fluorescence Probe Applications. *Adv. Opt. Mater.* **2015**, *3*, 112−119.
(24) Schmidt, L. C.; Pertegás, A.; González-Carrero, S.; Malinkiewicz, O.; Agouram, S.; Mínguez Espallargas, G. E.; Bolink, H. J.; Galian, R. E.; Pérez-Prieto, J. Nontemplate Synthesis of CH3NH3PbBr3 Perovskite Nanoparticles. *J. Am. Chem. Soc.* **2014**, *136*, 850−853.
(25) González-Carrero, S.; Galian, R. E.; Pérez-Prieto, J. Maximizing the Emissive Properties of $CH_3NH_3PbBr_3$ perovskite nanoparticles. *J. Mater. Chem. A* **2015**, *3*, 9187−9193.
(26) Zhu, R.; Zhao, Y.; Sun, T.; Liu, H.; Zhang, Y.; Li, X. The Impact of Trans/Cis Photoisomerization on Photoinduced Electron Transport between 4,4-Stilbenedicarboxylic Acid and Columnar Perylenediimide Aggregates in Water. *Colloid Polym. Sci.* **2015**, *293*, 2469−2475.
(27) Law, K. Y. Organic Photoconductive Materials: Recent Trends and Developments. *Chem. Rev.* **1993**, *93*, 449−486.
(28) Newman, C. R.; Frisbie, C. D.; da Silva Filho, D. A.; Brédas, J. L.; Ewbank, P. C.; Mann, K. R. Introduction to Organic Thin Film Transistors and Design of n-Channel Organic Semiconductors. *Chem. Mater.* **2004**, *16*, 4436−4451.
(29) Feng, J.; Zhang, Y.; Zhao, C.; Li, R.; Xu, W.; Li, X.; Jiang, J. Cyclophanes of Perylenetetraboxylicdiimide with Different Substituents at Bay Positions. *Chem. - Eur. J.* **2008**, *14*, 7000−7010.
(30) Knop, O.; Wasylishen, R. E.; White, M. A.; Cameron, T. S.; Oort, M. J. M. V. Alkylammonium Lead Halides. Part 2.$CH_3NH_3PbX_3$(X = Cl, Br, I) Perovskites: Cuboctahedral Halide Cages with Isotropic Cation Reorientation. *Can. J. Chem.* **1990**, *68*, 412−422.
(31) Sichert, J. A.; Tong, Y.; Mutz, N.; Vollmer, M.; Fischer, S.; Milowska, K.; Garcia-Cortadella, R.; Nickel, B.; Cardenas-Daw, C.; Stolarczyk, J. K.; Urban, A. S.; Feldmann, J. Quantum Size Effect in Organometal Halide Perovskite Nanoplatelets. *Nano Lett.* **2015**, *15*, 6521−6527.
(32) Poglitsch, A.; Weber, D. Dynamic Disorder in Methylammoium Trihalogenoplumbates (II) Observed by Millimeter-wave Spectroscopy. *J. Chem. Phys.* **1987**, *87*, 6373−6378.
(33) Li, C.; Liu, M.; Pschirer, N. G.; Baumgarten, M.; Müllen, K. Polyphenylene-Based Materials for Organic Photovoltaics. *Chem. Rev.* **2010**, *110*, 6817−6855.
(34) Cai, B.; Xing, Y.; Yang, Z.; Zhang, W.; Qiu, J. High Performance Hybrid Solar Cells Sensitized by Organolead Halid Perovskites. *Energy Environ. Sci.* **2013**, *6*, 1480−1485.

DOI: 10.1021/acs.langmuir.5b04221
Langmuir 2016, 32, 3294−3299